Lagrangian Eddy Trapping Fosters Chlorophyll Hot Spots in the North Pacific Subtropical Gyre

Alexandra E. Jones-Kellett[1,2], **Michael J. Follows**[1]

[1]Department of Earth, Atmospheric, and Planetary Sciences, Massachusetts Institute of Technology, Cambridge, MA, USA
[2]Biology Department, Woods Hole Oceanographic Institution, Woods Hole, MA, USA

Key Points:

- Mesoscale eddy trapping of chlorophyll is quantified using Lagrangian coherency metrics over feature lifetimes, from genesis to decay.
- Sea level anomaly eddies mix laterally with outside waters, resulting in weaker chlorophyll anomalies than within coherent eddies.
- The chlorophyll signature of eddy trapping differs regionally within a gyre, seasonally, by eddy age, and between cyclones and anticyclones.

Corresponding author: Alexandra E. Jones-Kellett, `jonesae@mit.edu`

Abstract

Vertical motions associated with mesoscale ocean eddies modulate the light and nutrient environment, stimulating phytoplankton biomass and chlorophyll anomalies. Populations within eddies may be trapped by the horizontal circulation or laterally diluted by mixing with surrounding waters. Conventionally, eddy boundaries are determined using Eulerian methods from daily satellite sea level anomaly fields. However, Eulerian methods do not delineate the bounds of trapped water masses, which is important to consider when interpreting eddy-induced changes in chlorophyll concentration. Integrated Lagrangian particle tracking methods, on the other hand, more accurately identify coherent structure boundaries that trap fluid masses for time scales relevant to phytoplankton bloom evolution. From two decades of remote sensing observations in the North Pacific Subtropical Gyre, we compared coincident Eulerian and Lagrangian eddy atlases to assess the impact of eddy trapping on chlorophyll concentration. We found more positive chlorophyll anomalies within Lagrangian coherent vortices than in Eulerian eddy boundaries and outside-eddy waters. Yet, there are striking differences seasonally and regionally within the gyre. Chlorophyll is most enriched within coherent boundaries of the Hawaiian Lee eddies and in the region southeast of the Islands in fall and winter. Our results suggest that typical Eulerian analyses underestimate the role of mesoscale eddies in enhancing chlorophyll by not accounting for lateral mixing. Consequently, quantifying the contribution of mesoscale eddies toward open ocean primary production is more complex than previously assumed.

Plain Language Summary

Mesoscale eddies are rotating ocean currents up to hundreds of kilometers in diameter. While some eddies continuously mix with their surroundings, referred to as leaky or dispersive, others are coherent and trap their constituents. Phytoplankton are free-floating microbes and their local concentrations are affected by the motions of these currents. The pigment chlorophyll enables phytoplankton to photosynthesize, which changes the ocean color and can be measured from space. We used satellite datasets and simulations of currents in the North Pacific to examine the effect of eddy coherency on phytoplankton concentration. We found coherent eddies trap phytoplankton, harboring greener waters than leaky eddies. In dispersive eddies, anomalous chlorophyll concentrations are diluted by mixing with surrounding waters. Thus, studies that do not quantify eddy trapping may underestimate the role of eddies in stimulating phytoplankton growth, which has implications for the global carbon budget. We also show that the chlorophyll signature of eddy trapping can vary regionally, seasonally, and as a function of eddy age. Most significantly, to the south of the Hawaiian Islands, we observed greener waters in coherent eddies than in their leaky counterparts in the fall and winter, signatures that are sustained over feature lifetimes.

1 Introduction

The North Pacific Subtropical Gyre (NPSG) maintains low phytoplankton biomass but is subject to high ecosystem variability (Karl & Church, 2017). Mesoscale eddies contribute to this variability, bringing nutrient-rich deep waters into the sunlit surface and stimulating phytoplankton growth in a temporary, quasi-isolated, altered environment. Eddies in the NPSG, including at Station ALOHA and the Hawaiian Lee Eddies, are the focus of seminal works describing biophysical interactions. For example, observations show that eddies affect biogeochemical cycling by enhancing primary production (Falkowski et al., 1991; Allen et al., 1996; Seki et al., 2001; Chen et al., 2008; Landry et al., 2008; McAndrew et al., 2008; Nicholson et al., 2008), modifying phytoplankton community structure (Olaizola et al., 1993; Vaillancourt et al., 2003; Brown et al., 2008; Fong et al., 2008; Barone et al., 2019; Harke et al., 2021), and intensifying carbon export (Bidigare et al.,

2003; Benitez-Nelson et al., 2007; Rii et al., 2008; Zhou et al., 2021; Barone et al., 2022). The NPSG, and analogous gyres in other basins, represent ecosystems of globally important scale, so the integrated effects of mesoscale biophysical interactions therein may play a significant role in Earth's carbon cycle.

1.1 Satellite Chlorophyll Signature of Eddies

Continuous satellite remote sensing of the Sea Level Anomaly (SLA) and chlorophyll-*a* (chl-*a*; a proxy for phytoplankton biomass) reveals significant relationships between ocean color anomalies and mesoscale eddies in global subtropical waters (Gaube et al., 2014; Dufois et al., 2016; He et al., 2016; Huang et al., 2017; Xu et al., 2019; Travis & Qiu, 2020). Yet, these relationships are complex; they differ regionally, seasonally, and between cyclonic and anticyclonic eddy polarities (see review by McGillicuddy Jr. (2016) and references therein). Cyclonic eddies in the Northern Hemisphere rotate counter-clockwise, depress the sea level, and shallow density surfaces. Eddy pumping in cyclones vertically displaces nutrient-rich deep waters into the euphotic zone, increasing phytoplankton biomass and surface chl-*a*. On the other hand, eddy-induced Ekman pumping can drive downwelling in the center of cyclones and decrease chl-*a*.

In contrast to cyclones, anticyclones in the Northern Hemisphere rotate clockwise, locally increase the sea level, and deepen isopycnals, which can reduce nutrient availability and decrease biomass. Other processes elevate biomass in subtropical anticyclones, including Ekman suction and winter convective mixing that vertically displaces nutrients into the mixed layer (Dufois et al., 2016). The vertical displacements of density surfaces in mesoscale eddies of either polarity can also cause phytoplankton cells to adjust their pigment content to adapt to differing light levels, further altering chlorophyll concentrations (Cornec et al., 2021; He et al., 2021; Strutton et al., 2023). These various mechanisms can result in anomalous concentrations of chl-*a* in subtropical gyre anticyclones and cyclones compared to outside-eddy waters.

1.2 Eddy Trapping

The horizontal circulation of mesoscale eddies can "trap" the signature of vertically-driven perturbations to phytoplankton biomass, acting to localize blooms (Gower et al., 1980; Provenzale, 1999; Fennel, 2001; Condie & Condie, 2016; He et al., 2022) and even preserve them as features transit across ocean basins (Lehahn et al., 2011; Villar et al., 2015). Eddy trapping is anticipated to garner monopoles of anomalous chl-*a* in eddy centers. However, it is still a challenge to disentangle from space-based observations whether mesoscale anomalies are signatures of actively changing biomass due to vertical processes or an advected, preserved plankton patch (Gaube et al., 2014).

Eddy trapping has major ecological implications. For example, coherent eddies formed near the Hawaiian coastline affect larval recruitment by trapping and transporting waters offshore (Vaz et al., 2013). Lateral trapping can also modulate trophic interactions (d'Ovidio et al., 2013; Lehahn et al., 2017) and alter phytoplankton community diversity by separating populations and sheltering them from competition (Bracco et al., 2000; Bastine & Feudel, 2010; Perruche et al., 2011; Clayton et al., 2013; Lévy et al., 2014; Hernández-Carrasco et al., 2023). So, coherent eddies may foster fluid dynamical niches (d'Ovidio et al., 2010; Lévy et al., 2015; Vortmeyer-Kley et al., 2019).

Individual eddies have varying trapping strengths, but censuses of the satellite chl-*a* response to eddies have not directly addressed the effects of this variability. The boundaries of mesoscale eddies are commonly detected using Eulerian metrics, for example from the SLA by assuming geostrophic balance (Chelton et al., 2011), and are often presumed to trap water masses. However, studies consistently find that Eulerian-detected boundaries are not necessarily materially coherent (Beron-Vera et al., 2013; Haller & Beron-

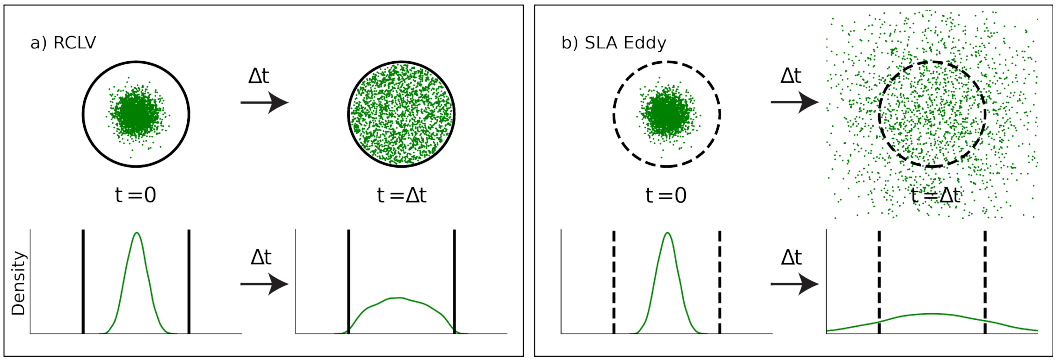

Figure 1. Schematic of the fates of phytoplankton blooms in coherent and leaky eddies. **(a)**, **(b)** At $t = 0$, identical blooms are induced by the eddies. **(c)** At $t = \Delta t$, phytoplankton cells in the coherent eddy are distributed within the boundaries, but in-eddy waters do not mix with surrounding waters. **(d)** At $t = \Delta t$, the bloom in the leaky eddy is diluted via mixing with outside-eddy waters. This resulted in a lower biomass concentration than in the coherent eddy, despite the initial generation of an equivalent bloom.

Vera, 2013; Y. Wang et al., 2015; Beron-Vera et al., 2019; T. Liu et al., 2019; Andrade-Canto et al., 2020; Katsanoulis et al., 2020; T. Liu et al., 2022; Denes et al., 2022). In fact, only 54% of SLA eddies in the NPSG contain a coherent structure of substantial size that persists for at least a month (Jones-Kellett & Follows, 2024). This suggests that waters along SLA eddy boundaries mix with surrounding waters, and for many, the entire eddy structure is dispersive.

By delineating between coherent and "leaky" eddies, we can better understand the magnitudes and fates of eddy-driven biogeochemical perturbations. Figure 1 schematically demonstrates the outcome of equivalent phytoplankton blooms generated in a (a) coherent and (b) leaky eddy. After the initial blooms are diluted for time Δt, the coherent eddy maintains a more highly concentrated population than the leaky eddy because the cells cannot escape the bounds. We anticipate that such eddy-driven anomalies will dissipate as eddies age due to lateral dilution (although this process is slowed in a coherent eddy), vertical dilution, or ecological dynamics such as grazing or the reduction of nutrient availability.

Here we address two hypotheses: (i) Coherent eddies are more likely to contain "hot spots" of chlorophyll relative to the climatological mean field by suppressing lateral dilution of eddy-driven anomalies. (ii) Eddy chlorophyll anomalies, relative to their immediate surroundings, will decline with eddy age even in the most coherent features.

1.3 Overview

Lagrangian methods accurately measure eddy coherency in a time-varying flow (Haller, 2015). Interpreting biophysical interactions in a Lagrangian sense follows naturally, since phytoplankton experience a moving reference frame (Woods & Onken, 1982; Lehahn et al., 2018). To test the hypothesis that Lagrangian coherent vortices contain elevated chl-*a* concentrations compared to leaky, Eulerian eddies, we analyzed two decades of satellite observations and the development of eddy boundaries in the NPSG. We compared an SLA eddy atlas with a complementary Lagrangian coherent eddy atlas built for biogeochemical applications in Section 2.1. Section 3.1 evaluates an overall elevation of surface chl-*a* due to eddy trapping in the gyre. Key seasonal and sub-regional differences

in the biological response to eddy trapping are revealed in Section 3.2. Lastly, Section 3.3 examines the evolution of chl-a anomalies in vortices that maintain coherency for five or more months. Our results suggest that perturbations in biomass triggered by eddies may be underestimated when lateral mixing and dilution are not accounted for.

2 Materials and Methods

The study domain extends from 2000 to 2019 and the region 15-30°N, 180-230°E (see the box in Fig. 2a). We selected these spatial bounds to reduce the degrees of freedom associated with large-scale environmental variability from the ultra-oligotrophic western NPSG, Transition Zone Chlorophyll Front (Glover et al., 1994), California Current System, and equatorial currents. Focusing on this area of the gyre enabled us to comprehensively evaluate sub-regional and seasonal patterns in the chlorophyll signatures of eddy trapping. We used the Copernicus Marine Service (CMEMS) 1/4° daily satellite geostrophic current and SLA gridded fields for Eulerian and Lagrangian eddy identification (CMEMS, 2020). We obtained the 8-day averaged satellite chl-a Ocean Color Climate Change Initiative (OC-CCI) product with a spatial resolution of $4km$ at the equator (Sathyendranath et al., 2019).

2.1 Eddy Atlases

2.1.1 Eulerian Eddy Atlas

We used the OceanEddies algorithm to generate an Eulerian eddy atlas from the satellite SLA (Faghmous et al., 2015). The flexible software allowed us to set parameters aligned as closely as possible to the Lagrangian eddy atlas, described in Section 2.1.2. OceanEddies identifies an eddy boundary as the outermost closed contour containing a single SLA extremum and tracks the movement of feature over time. We required eddies to have a minimum detectable lifespan of 32 days and boundaries to contain twelve or more 1/4° grid cells. The smallest SLA eddy from this criteria has an area of $8,048km^2$ with a radius of approximately $50km$, consistent with the Rossby radius of deformation in the domain (Chelton et al., 1998). We set the eddy disappearance parameter to 3 days, which accounts for noise in the gridded SLA satellite product that could cause a premature termination to eddy tracking. We reduced the temporal resolution of the SLA atlas to an 8-day frequency, synchronized with the OC-CCI chl-a product, for the ensuing analysis. From two decades of data, we tracked 6,846 unique SLA eddies (or 52,553 observations resolved every 8 days), including 3,322 anticyclones characterized by SLA maxima and 3,524 cyclones characterized by SLA minima.

2.1.2 Lagrangian Eddy Atlas

We expanded upon the Lagrangian eddy atlas developed by Jones-Kellett and Follows (2024) to identify and track coherent vortices. Eddy boundaries were derived from the Lagrangian Averaged Vorticity Deviation (LAVD), a measure of the integrated vorticity experienced by a Lagrangian particle over a timescale of interest (Haller et al., 2016). First, the LAVD for Lagrangian particles is mapped to their gridded initialization locations. Closed contours surrounding a local maximum in the resulting LAVD field are assumed to be fluid sets in rigid-body rotation, referred to as Rotationally Coherent Lagrangian Vortices (RCLVs) (Haller et al., 2016; Tarshish et al., 2018). Then, RCLVs that maintained coherency for at least 32 days were tracked through time and space at an 8-day resolution using backward-in-time particle simulations synchronized with the OC-CCI 8-day chl-a product (Fig. S1).

Young, developing eddies can harbor large biological anomalies (Gaube et al., 2013). So to holistically evaluate how eddy trapping alters chl-a concentration, it was important to resolve RCLV genesis. The RCLV atlas presented by Jones-Kellett and Follows

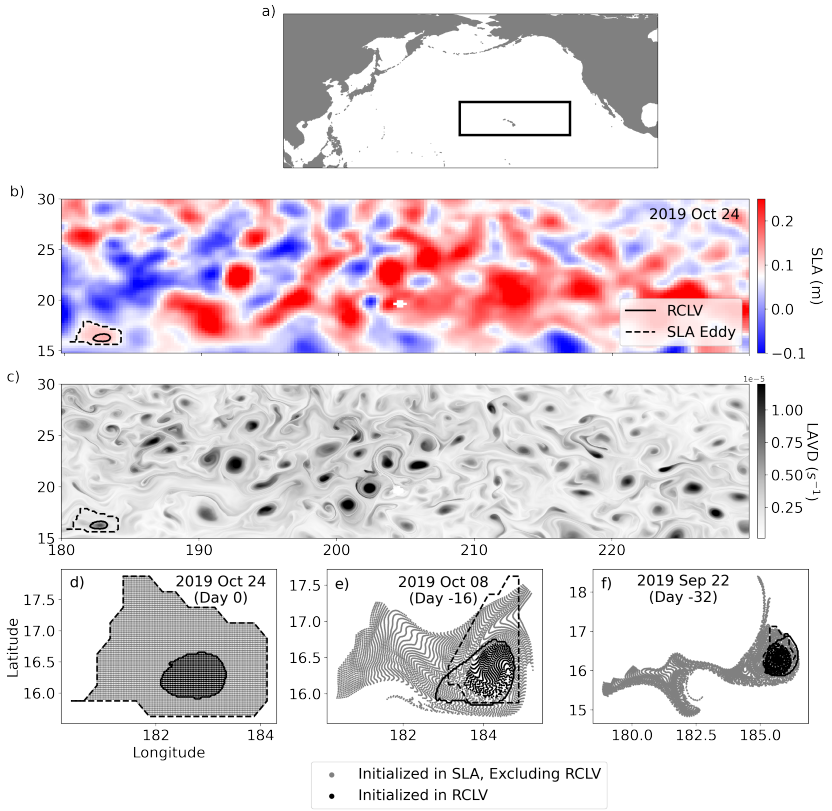

Figure 2. **(a)** The North Pacific Ocean, where the black box outlines the bounds of the subtropical gyre domain that is the focus of this study. **(b)** The SLA field on 24 October 2019, with the boundaries of one eddy overlaid. The black dotted contour represents the SLA eddy boundary, and the black solid contour is the Rotationally Coherent Lagrangian Vortex (RCLV) boundary. **(c)** The Lagrangian Average Vorticity Deviation (LAVD) field on 24 October 2019, with the same eddy boundaries as in (b) overlaid. **(d-f)** The advection of Lagrangian particles, moving backward-in-time from left to right. **(d)** Lagrangian particles were initialized inside the SLA (gray and black) and RCLV (black) boundaries on 24 October 2019. The gray particles are categorized as "SLA excluding RCLV". **(e)** The particle locations on 8 October 2019, or 16 days backward-in-time from the initialization date, and **(f)** on 22 September 2019, or 32 days backward-in-time. The evolving SLA (dotted contour) and RCLV (solid contour) eddy boundaries are overlaid for each corresponding date.

(2024) (Jones-Kellett, 2023a) included features that were above a size threshold and coherent for at least 32 days. In other words, the youngest eddies captured in Version 1 are already 32 days old. Here, we initialized Lagrangian particles in each 32-day-old RCLV and tracked them backward in time with the OceanParcels software (Delandmeter & van Sebille, 2019) to 8 days of age. Following the existing atlas resolution, at 8-day timesteps (ages 24, 16, and 8), we drew closed contours to encompass the particle set (Fig. S2). The quality control steps conducted for the extended RCLV atlas are detailed in the decision tree in Fig. S3. This new version of the RCLV atlas (Jones-Kellett, 2024) contains 11,855 unique RCLVs (or 75,445 polygons resolved every 8 days), including 5,592 anticyclones characterized by a negative sign of relative vorticity and 6,263 cyclones characterized by a positive sign of relative vorticity.

The animation supplement shows the space-time evolution of (a) RCLVs overlaid on the LAVD fields that they were derived from and (b) SLA eddies overlaid on the SLA for the year 2010. Panel (c) shows the boundaries of both eddy types overlaid on the climatological chl-a anomaly (Eq. 1).

2.2 Eddy Categorization

When comparing RCLVs and SLA eddies from concurrent atlases, it is notable that some features are observed with only one method whereas many are detected with both (T. Liu et al., 2019). However, when eddies are identified in both datasets, the boundaries can differ considerably. "Overlapping" RCLVs tend to be nested within a larger SLA eddy boundary, so waters associated with SLA eddies or RCLVs are not necessarily mutually exclusive (Jones-Kellett & Follows, 2024).

We categorized each pixel from the satellite chl-a fields as background (i.e., outside-eddy) or inside an eddy. In-eddy pixels can be within an SLA eddy, RCLV, or both. Pixels inside an SLA eddy boundary but not an RCLV are referred to as "SLA excluding RCLV". This includes the dispersive regions of overlapping eddies (i.e., the gray particles in Fig. 2d) and the entirety of SLA eddies that do not contain a coherent structure. The "SLA eddy" category includes all pixels within an eddy boundary irrespective of whether it contains an RCLV (i.e., the gray *plus* the black particles in Fig. 2d). This classification is directly comparable to studies that invoke Eulerian eddy identification methods. Figure 2d-f demonstrates the considerable difference in the trapping nature of the respective eddy identification methods. The black particles initialized in the RCLV remain inside the eddy after advection backward through time, whereas many gray particles initialized in the SLA eddy are not associated with the feature only 16 days prior.

2.3 Chlorophyll Anomaly Definitions

The climatological chl-a anomaly is a temporal, Eulerian metric defined

$$\delta c_{clim}(x,y,t) = c(x,y,t) - \frac{1}{M}\sum_{t'=0}^{M} c(x,y,t') \tag{1}$$

where $c(x,y,t)$ is the chl-a at location (x,y) and time t. The second term describes the 2000 to 2019 average chl-a in the month corresponding to the date t (i.e., the monthly climatology shown in Fig. S4), such that M is the number of data points available for that month. A positive δc_{clim} indicates that chl-a is higher than the average at that location in the given month. We used δc_{clim} to isolate the mesoscale-driven changes in chl-a that are distinct from the seasonal cycle.

We define the relative difference in the eddy and background probability density distributions of δc_{clim} as

$$f(\delta c_{clim}) = \frac{p_E(\delta c_{clim}) - p_B(\delta c_{clim})}{p_B(\delta c_{clim})}. \tag{2}$$

$p_E(\delta c_{clim})$ is the density distribution of the climatological chl-a anomalies in an eddy type and $p_B(\delta c_{clim})$ is the density distribution of anomalies in the background ocean. $f(\delta c_{clim})$ is the likelihood of observing a given chlorophyll anomaly in waters sampled in the eddy type versus the background. For example, $f(\delta c_{clim}) > 0$ indicates the given value of δc_{clim} is more likely to be observed in an eddy than outside.

The local, eddy-associated chl-a anomaly is defined

$$\delta c_{loc} = \underbrace{\frac{1}{A_{in}} \oint_I c(x,y)\, dI}_{\text{Inside Eddy}} - \underbrace{\frac{1}{A_{out}} \oint_O c(x,y)\, dO}_{\text{Outside Eddy}} \tag{3}$$

where I is the eddy polygon with area A_{in}, and O is the annulus from the eddy boundary to double the eddy radius with area A_{out}. The first term of Eq. 3 is the average chl-a inside the eddy and the second is the average in the immediate surroundings. A positive δc_{loc} indicates that the mean chl-a concentration is higher within the eddy than outside. Since this metric follows an eddy through time and space, it can be considered a Lagrangian chl-a anomaly.

3 Results

3.1 Chlorophyll Signatures of Eddy Trapping

To isolate eddy-driven changes in chl-a, we removed the seasonality at each grid cell in the satellite chl-a fields (Eq. 1), yielding climatological chl-a anomaly fields from 2000 to 2019. We binned the climatological chl-a data by the categorizations described in Section 2.2: Anticyclonic RCLV, Anticyclonic SLA eddy, Anticyclonic SLA excluding RCLV, Cyclonic RCLV, Cyclonic SLA eddy, Cyclonic SLA excluding RCLV, or background. Background chlorophyll observations are outside of all eddy types.

3.1.1 Anticyclonic Eddies

Anticyclonic eddies alter chlorophyll concentrations in the NPSG. Figure 3a shows the probability density distributions of the chl-a anomaly relative to the seasonal climatology (δc_{clim}) for anticyclones (in red) and the background ocean (in gray). The quantiles of the distributions (indicated by the dots in Fig. 3a) consistently shift toward higher δc_{clim} in RCLVs compared to SLA eddies. The distribution of δc_{clim} in RCLVs is also shifted more positively relative to the background ocean except at the 99% quantile. These results suggest that anticyclonic eddy trapping elevates chl-a in the NPSG.

To further disentangle how the eddies alter surface chlorophyll, we plotted $f(\delta c_{clim})$ in Fig. 3b. This metric quantifies whether a given δc_{clim} is more likely to be observed in randomly sampled waters of the background ocean or an eddy. Each quadrant of the figure can be interpreted as follows:

- Q1: **Positive** anomalies are **more likely** to be observed in an eddy than in the background ($f(+\delta c_{clim}) > 0$).
- Q2: **Negative** anomalies are **more likely** to be observed in an eddy than in the background ($f(-\delta c_{clim}) > 0$).
- Q3: **Negative** anomalies are **less likely** to be observed in an eddy than in the background ($f(-\delta c_{clim}) < 0$).
- Q4: **Positive** anomalies are **less likely** to be observed in an eddy than in the background ($f(+\delta c_{clim}) < 0$).

Negative values of δc_{clim} are less likely to occur within all anticyclonic eddy types than in the background (Fig. 3b: Q3). Positive chl-a anomalies are more common in all anticyclonic eddy types compared to outside eddies (Fig. 3b: Q1), except at extremely

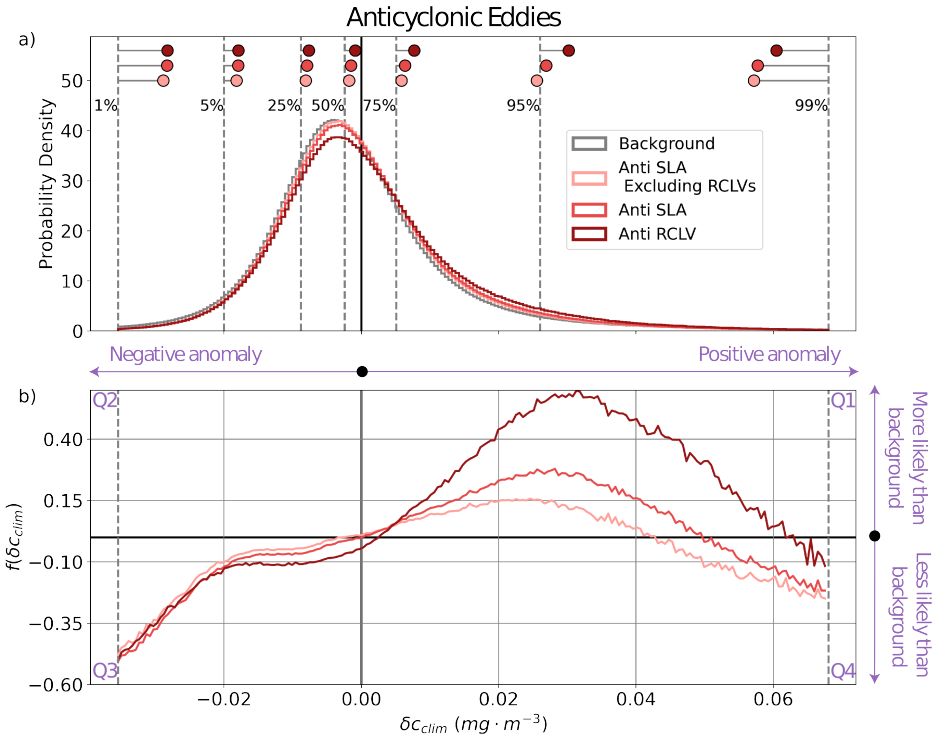

Figure 3. **(a)** The histograms depict the probability density distributions of the climatological chl-a anomalies (δc_{clim}; Eq. 1) in anticyclones from the 1 – 99% quantiles. The vertical, dotted gray lines depict the quantiles of the background distribution. The dots show the equivalent quantiles for each eddy category, demonstrating the shifts in the distributions from the background. **(b)** The relative difference in the anticyclonic eddy density distribution from the background density distribution ($f(\delta c_{clim})$; Eq. 2) plotted from the 1 to 99% quantiles (i.e., the gray dotted lines). A positive $f(\delta c_{clim})$ indicates that the given δc_{clim} is more likely to be observed when sampling an in-eddy water parcel than when sampling the background.

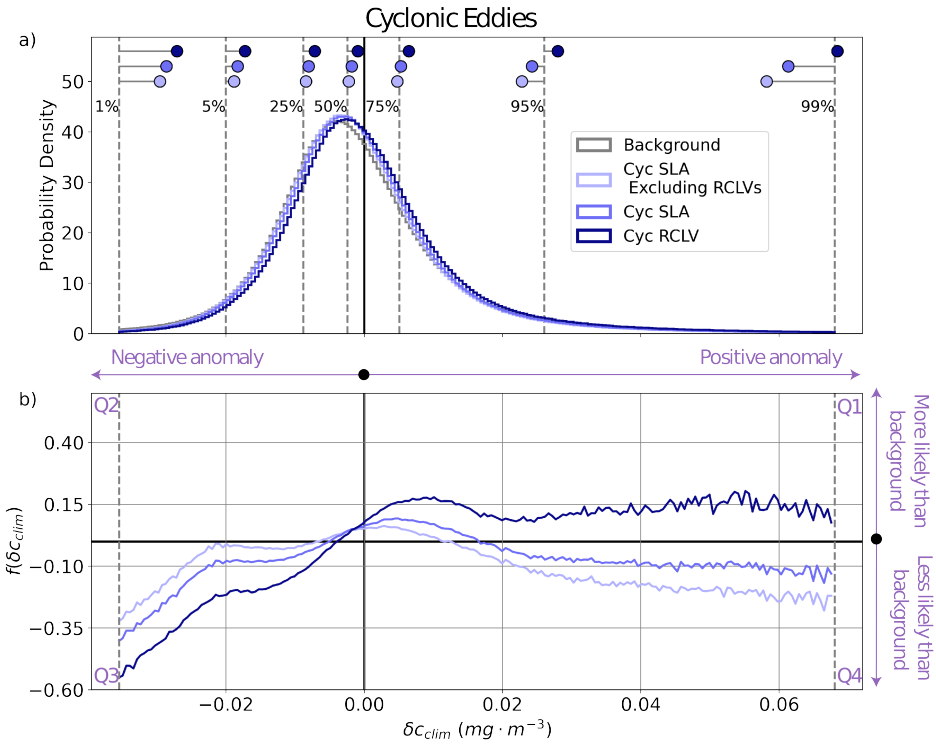

Figure 4. Same as Figure 3, but for cyclonic eddies. **(a)** The histograms depict the probability density distributions of the climatological chl-a anomalies (δc_{clim}; Eq. 1) in cyclones from the 1 – 99% quantiles. The vertical, dotted gray lines depict the quantiles of the background distribution. The dots show the equivalent quantiles for each eddy category, demonstrating the shifts in the distributions from the background. **(b)** The relative difference in the cyclonic eddy density distribution from the background density distribution ($f(\delta c_{clim})$; Eq. 2) plotted from the 1 to 99% quantiles (i.e., the gray dotted lines). A positive $f(\delta c_{clim})$ indicates that the given δc_{clim} is more likely to be observed when sampling an in-eddy water parcel than when sampling the background.

high values (Fig. 3b: Q4). More specifically, anomalies over 0.0504 $mg{\cdot}m^{-3}$ occurring in SLA eddies and 0.0631 $mg{\cdot}m^{-3}$ in RCLVs are rarer than in the background. Therefore, anticyclones elevate chl-a up to a certain threshold.

21% of satellite pixels co-located within anticyclonic SLA eddies are also contained within an RCLV (Table S2). In other words, only a fifth of the aggregate SLA eddy area is coherent timescales on the order of months. The leaky zones of SLA eddies, or SLA excluding RCLVs, are more likely than the background to contain positive δc_{clim}, but only up to 0.0424 $mg{\cdot}m^{-3}$. This threshold is lower than for RCLVs and the all-inclusive SLA eddy categories, indicating that the highest chl-a anomalies associated with SLA eddies are largely contained within nested Lagrangian coherent structures.

3.1.2 Cyclonic Eddies

Cyclonic eddies alter surface chlorophyll in the NPSG compared to outside-eddy waters with signatures that differ in some ways from anticyclones. Negative climatological anomalies are less likely to occur in all cyclonic eddy types than in the background ocean and least likely in RCLVs (Fig. 4b: Q3), as was the case for anticyclones. Cyclonic

RCLVs are likelier to have positive chl-a anomalies than the background ocean (Fig. 4b: Q1). However, unlike anticyclonic RCLVs, cyclonic coherent structures elevate chl-a to, or maintain chl-a, even at very high values. Yet, moderately positive δc_{clim} are less likely to occur in cyclones (Fig. 4b: Q1) compared to anticyclones (Fig. 3b: Q1). Other than for very modest values ($< 0.016\ mg \cdot m^{-3}$), SLA cyclones are less likely to have positive chl-a anomalies than the background (Fig. 4b: Q1, Q4). 23% of satellite pixels in cyclonic SLA eddies are also contained within an RCLV (Table S3) and are not included in the "SLA eddies excluding RCLVs" category. The leakiest components of SLA eddies are less likely than the background to contain a positive chlorophyll anomaly greater than $0.0117\ mg{\cdot}m^{-3}$. Hence, in both cyclones and anticyclones, coherent structures within SLA eddies are more often associated with positive chl-a anomalies than the background ($\delta c_{clim} > 0$).

In summary, RCLVs of both polarities are less likely to have negative chl-a anomalies and more likely to have positive anomalies compared to the background and SLA eddies. Fewer positive chl-a anomalies are attributed to SLA eddies when excluding nested RCLVs than to all-encompassing SLA eddies. This supports the hypothesis that phytoplankton blooms are rapidly diluted via lateral mixing when coherent structures do not trap and preserve the eddy-driven biological perturbations.

3.2 Regional and Seasonal Subdomains

Further examination reveals significant regional and seasonal variations in the role of eddy trapping toward altering chl-a concentrations in the NPSG. Subdomains of contrasting mesoscale eddy character can be defined using the eddy polarity probability (P) (Chaigneau et al., 2009), defined

$$P(x,y) = \frac{F_A(x,y) - F_C(x,y)}{F_A(x,y) + F_C(x,y)}. \tag{4}$$

$F_A(x,y)$ ($F_C(x,y)$) is the number of times the pixel at location (x,y) was inside an anticyclone (cyclone) from 2000 to 2019. Anticyclonic eddy polarity is more frequent than cyclonic when $P > 0$. Figure 5a depicts the geographic distribution of P for RCLVs, revealing more anticyclonic activity north of 23°N, cyclonic domination to the southeast of Hawai'i, and signatures of the Lee eddies to the west of the islands. We found distinct and sometimes dramatic differences in the chl-a responses between anticyclonic and cyclonic eddies of the north, southeast, and Hawaiian Lee provinces. The monthly chl-a climatologies vary moderately by region (Fig. S5).

3.2.1 Northern Eddies

In the winter and spring (Fig. 5b, d) there are no substantial disparities in chl-a anomalies between northern RCLVs and SLA eddies. However, some differences emerge in the summer and fall (Fig. 5f, h), indicating an influence of eddy trapping on chlorophyll patchiness in the surface ocean. Although Section 3.1 documents an overall increase in positive chl-a anomalies within RCLVs compared to SLA eddies, there are exceptions to this pattern in the north province. This emphasizes the need for focused regional and seasonal analyses and illustrates the complexity of biogeochemical response to mesoscale eddies.

Occurrences of positive δc_{clim} are more common in all types of anticyclones (represented by the red curves in Fig. 5) than in the background during the northern fall and winter, up to approximately $0.0555\ mg{\cdot}m^{-3}$ in the winter and $0.0394\ mg{\cdot}m^{-3}$ in the fall. This aligns with global observations of elevated surface chl-a in wintertime anticyclonic eddies in subtropical gyres (Dufois et al., 2016). During the summer and fall, anticyclonic RCLVs, but not SLA eddies, are likelier to have a negative chl-a anomaly than the background. This suggests that, in some cases, limited dilution in RCLVs yields a

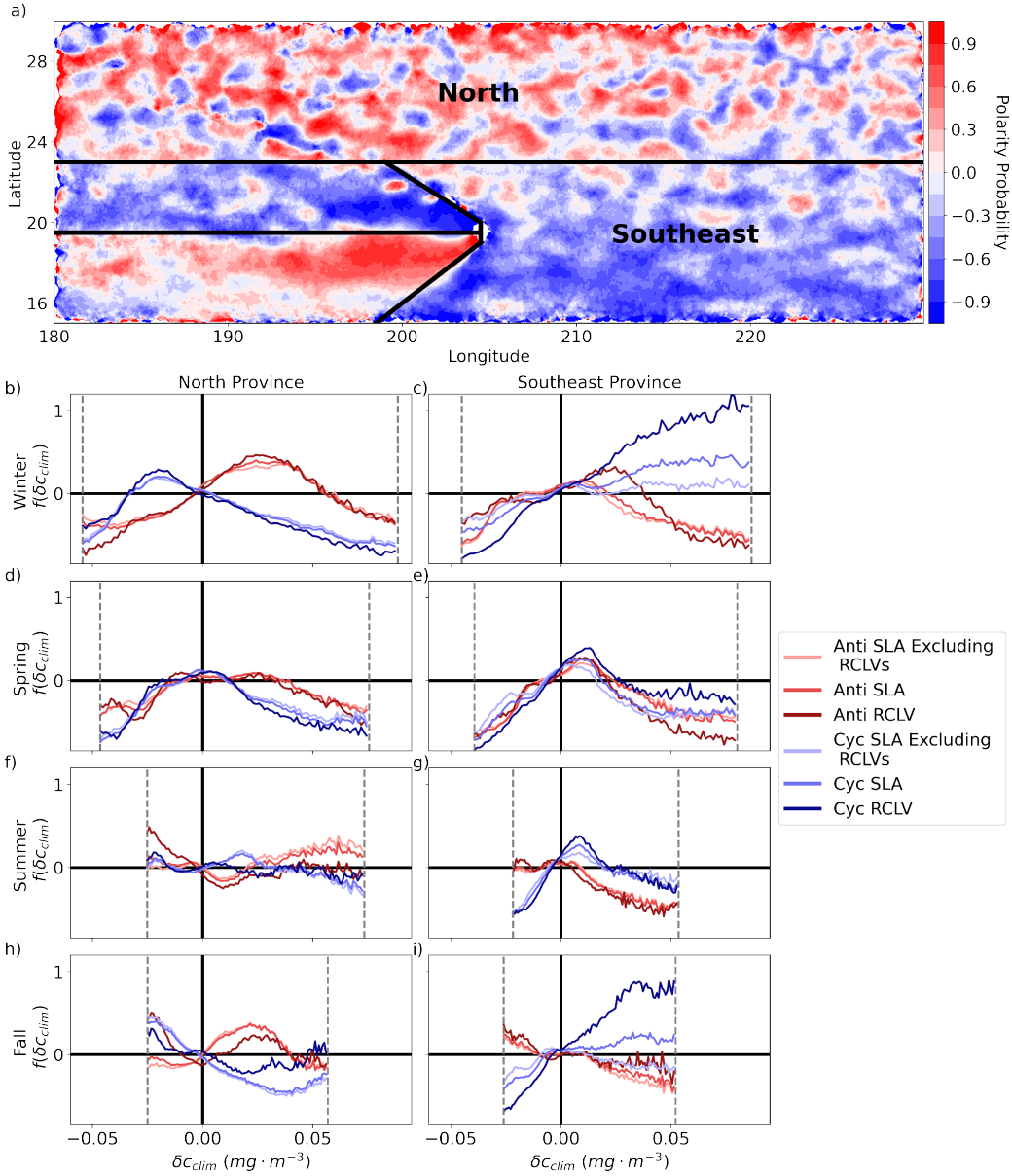

Figure 5. **(a)** RCLV polarity probability (Eq. 4). Red (blue) indicates that anticyclones (cyclones) are more common at the location. The black lines delineate mesoscale-driven provinces as defined in this study. **(b-i)** The relative difference in the probability density distribution of the climatological chl-a anomaly (δc_{clim}) from the background ($f(\delta c_{clim})$) for each eddy type. Each row corresponds with a season such that winter includes December through February. The dotted gray lines show the 1-99% quantiles of the background ocean for the season and region. These are the cutoff boundaries of the curves so that there is sufficient data underlying the calculations of $f(\delta c_{clim})$. Figures S6 and S7 show the corresponding probability density distributions.

local depletion of chl-a. On the other hand, SLA anticyclones have $f(\delta c_{clim}) > 0$ for more positive values of δc_{clim} than RCLVs in the summer and fall, indicating that eddy edge processes are responsible for enhancing chl-a concentrations within SLA-derived boundaries during these seasons.

Northern cyclonic eddies (represented by the blue curves in Fig. 5) generally exhibit fewer positive chl-a anomalies than the background across all seasons except the summer, where the distributions resemble the background ocean. Moreover, cyclonic RCLVs are less prone to have positive anomalies than SLA eddies in all seasons except for the fall, indicating that eddy trapping does not typically heighten chlorophyll levels in cyclonic features of the northern province. In the winter and fall, northern cyclones of all types are likelier to display negative δc_{clim} values than the background.

3.2.2 Southeastern Eddies

The probability density distributions of δc_{clim} exhibit substantial disparities between RCLVs and SLA eddies within the southeast province, especially in cyclones, for all seasons (Fig. 5c, e, i) except for the summer (Fig. 5g). Notably, anticyclones are much less prevalent than cyclones in the southeast province, so observations of anticyclones in this region play a small role in their overall effects in the gyre shown in Fig. 3. Conversely, the high frequency of cyclones in the southeast contributes largely to the data in Fig. 4.

Southeastern anticyclonic eddies have distinct relationships with chl-a compared to their northern counterparts. In winter, anticyclonic RCLVs are more likely to exhibit positive δc_{clim} values but up to a lower threshold ($0.0374\ mg{\cdot}m^{-3}$) than in the northeast ($0.0542\ mg{\cdot}m^{-3}$). Unlike in the northeast, wintertime SLA anticyclones have distributions more akin to the background. During spring, all anticyclonic eddy types are likelier than the background to have small positive δc_{clim}, up to $0.02\ mg \cdot m^{-3}$. However, positive chl-a anomalies in southeastern anticyclones are unlikely in summer and fall, with all types in the fall showing a propensity for negative anomalies. This differs from the northern fall where positive δc_{clim} values are found in anticyclonic eddies and only RCLVs are likely to have negative anomalies.

Cyclonic δc_{clim} distributions in the southeast province differ greatly from the north. All cyclone types exhibit $f(\delta c_{clim}) < 0$ for negative δc_{clim} throughout the year, suggesting that cyclones consistently enhance chl-a in this region. During fall and winter, cyclonic RCLVs are much likelier than the background and SLA eddies to have positive δc_{clim}, especially at high values. Because the chl-a signatures of cyclonic SLA eddies excluding RCLVs are similar to the background, positive anomalies in the SLA eddies can be largely attributed to RCLVs nested within their bounds. Thus, eddy trapping plays a prominent role in elevating local chl-a anomalies in cyclones of the southeast province. During spring and summer, southeastern cyclones are more likely to have positive anomalies of δc_{clim} within certain thresholds. This cutoff is $0.0182\ mg{\cdot}m^{-3}$ for cyclonic SLA eddies in the spring and $0.0263\ mg{\cdot}m^{-3}$ for RCLVs. In summer, it is $0.0192\ mg{\cdot}m^{-3}$ for SLA eddies and $0.0246\ mg \cdot m^{-3}$ for RCLVs.

3.2.3 Hawaiian Lee Eddies

The "Hawaiian Lee Eddies" are large, long-lived features that consistently form in the Lee of the Hawaiian Islands (Fig. 6a). Anticyclones are generated by the shear instability between the eastward-flowing Hawaiian Lee Countercurrent and the westward-flowing North Equatorial Current (Calil et al., 2008; Yoshida et al., 2010; Y. Liu et al., 2012). Lee cyclones are produced from wind stress curl anomalies due to trade wind blocking by the islands (Lumpkin, 1998; Dickey et al., 2008; Yoshida et al., 2010). The Hawaiian Lee Countercurrent to the south and the westward-flowing Hawaiian Lee Current to

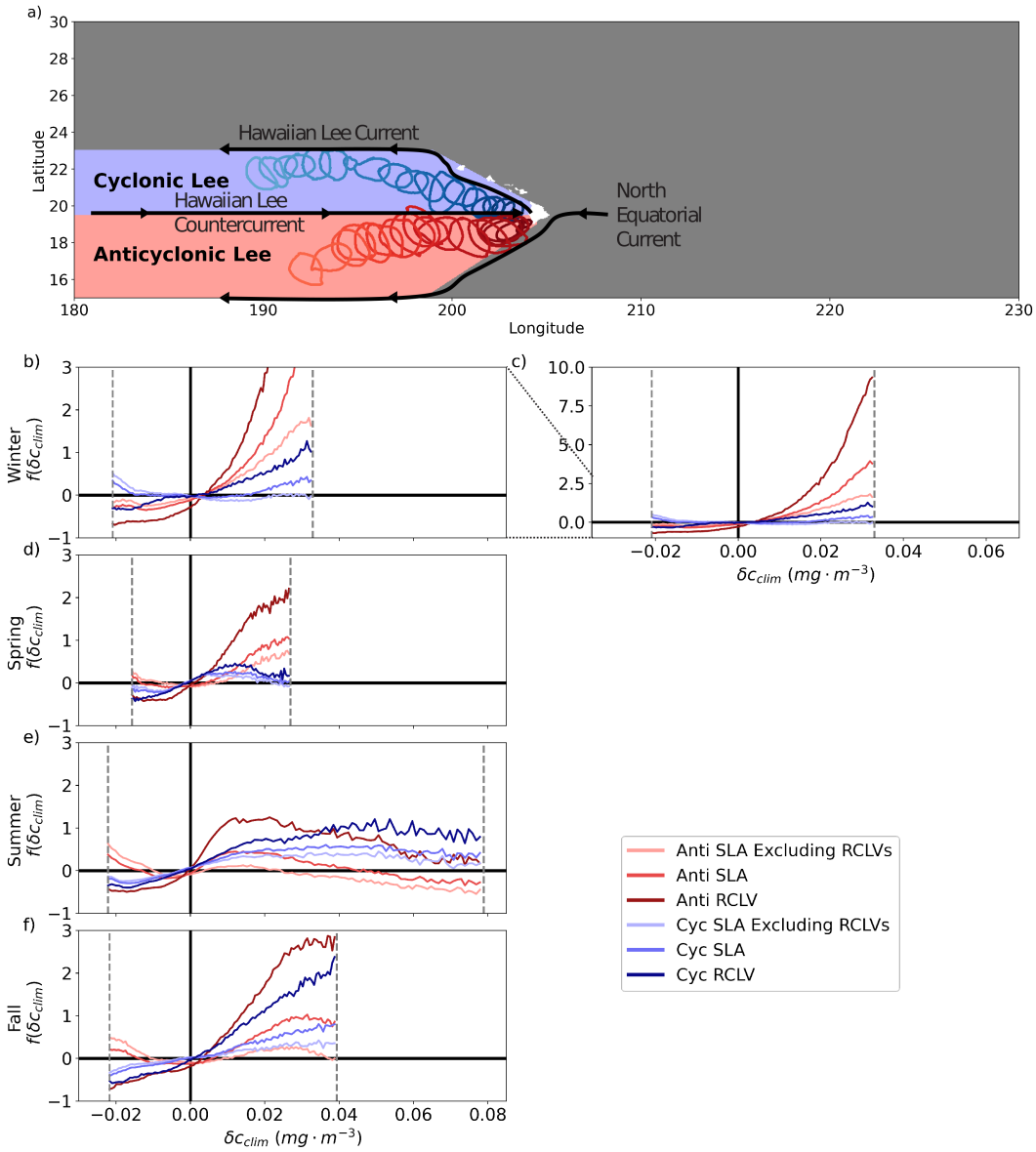

Figure 6. **(a)** Schematic of the currents that sustain the Hawaiian Lee Eddies. The region dominated by cyclones (anticyclones) is blue (red). The boundaries of two RCLVs are plotted every 16 days to show the common propagation pathways westward from the islands, where the darker contours represent young eddies and the lighter represent old eddies. **(b-f)** The relative difference in probability density distributions of the climatological chl-a (δc_{clim}) anomaly from the background ($f(\delta c_{clim})$)). The dotted gray lines show the 1-99% quantiles of the background ocean for the season and region. These are the cutoff boundaries of the curves so that there is sufficient data underlying the calculations of $f(\delta c_{clim})$. Figure S8 shows the corresponding probability density distributions. Note that the y-axis differs from Figs. 3, 4, and 5 to accommodate larger values of $f(\delta c_{clim})$. Panel **(c)** includes the same information as **(b)** with a different y-axis to expose the entirety of the curves.

the north sustain the cyclonic vorticity, evident from bands in the sign of polarity probability to the west of the Islands (Fig. 5a).

RCLVs and SLA Lee Eddies of both polarities drive more positive chlorophyll anomalies than the background throughout the entire annual cycle (Fig. 6b-f), distinguishing them from features examined in Sections 3.2.1 and 3.2.2. RCLVs of both polarities have more positive chl-a anomalies than their corresponding SLA eddies and the background across all seasons. SLA eddies excluding RCLVs more closely resemble the background, highlighting the importance of trapping for locally enhancing the chl-a signature of the Hawaiian Lee Eddies.

Although the chl-a anomalies of the Lee Eddies are consistently positive, the magnitudes vary seasonally. In summer and fall, δc_{clim} distributions are similar between cyclones and anticyclones, whereas, during the winter and spring, anticyclones are much more prone to positive anomalies. Even the leakiest anticyclonic features host positive δc_{clim} on par with cyclonic RCLVs during these seasons. Wintertime anticyclonic RCLVs host the most extreme positive δc_{clim} compared to all other eddies in the domain. Summer and fall witness more negative anomalies of chl-a in anticyclonic SLA eddies than in the background, suggesting that chl-a can also be depleted in these features. This is only the case for cyclonic SLA eddies in the winter.

To summarize the regional variations, the response to anticyclones and cyclones is different in the north, but there is less contrast between SLA and RCLV features, suggesting a weak role for trapping there. In the southeast, there are differences between chl-a anomalies in SLA and RCLV features, suggesting a stronger role for trapping. In the Lee of the Hawaiian Islands, cyclones and anticyclones elevate chl-a and there is a strong signature of trapping in the contrast between SLA and RCLV features.

3.3 Evolution of Long-lived Coherent Eddies

The RCLV atlas enables the examination of chl-a patches as they evolve through time as quasi-isolated systems. Accordingly, we analyzed the in-eddy anomaly compared to the immediate surroundings, δc_{loc} (Eq. 3), as a function of age for the 245 RCLVs (109 anticyclones, 136 cyclones) that maintained coherency for 150 or more days. Figure S9 illustrates the consistent westward propagation of these features.

Figure 7 shows the magnitude of the local, Lagrangian chlorophyll anomalies with age, separated by season and province. The results reject the initial hypothesis that anomalies would decline over eddy lifetimes, although this is sometimes true. There is not a single, consistent pattern of change in δc_{loc} with age, rather it depends on the region, season, and polarity, complimenting the results of Section 3.2. For example, RCLVs in the north have minimally altered chl-a compared to their immediate surroundings except in wintertime anticyclones, which show some elevation relative to their surroundings early in their lifetimes. Southeastern cyclonic RCLVs foster heightened chl-a relative to their surroundings in the winter and fall, and these anomalies do decline with eddy age, consistent with the initial hypothesis. Hawaiian Lee RCLVs, both cyclones and anti-cyclones, have dramatically enhanced chl-a relative to their surroundings throughout their lifetimes. Interestingly, δc_{loc} monotonically and substantially increases with eddy age in winter-time Lee Eddy anticyclones.

4 Discussion

Harnessing the temporal and spatial coverage of satellite observations, we measured the effects of mesoscale eddy trapping on chl-a in the NPSG over two decades. We compared Lagrangian (RCLV) and Eulerian (SLA) eddy atlases to differentiate the biological signatures of coherent eddies, dispersive eddies, and the background ocean. As hy-

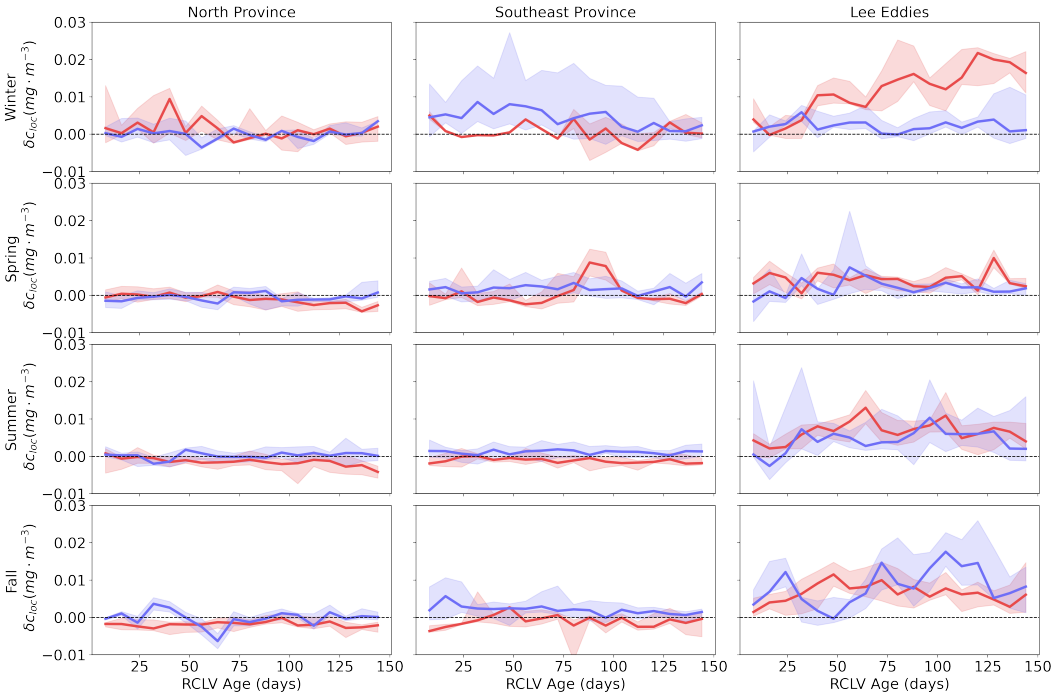

Figure 7. Local chl-a anomalies (δc_{loc}) in RCLVs with lifespans of 150+ days. Each column corresponds to a mesoscale-driven province and each row with the season. Cyclonic (anticyclonic) eddies are in blue (red). The solid lines show the median δc_{loc} by RCLV age, and the shaded areas are the ranges of the 25 to 75% quantiles.

pothesized, more positive climatological chl-a anomalies are observed in RCLVs than in SLA eddies or outside-eddy waters (Figs. 3, 4).

We find systematic regional and seasonal variations in surface chl-a anomalies in response to Lagrangian eddy trapping within the gyre (Figs. 5, 6). Notably, the modulation of chl-a differs between cyclones and anticyclones in the northern NPSG province, though the impact of trapping is weakest there. Chl-a is strongly altered by trapping in the southeastern region, particularly in the Hawaiian Lee Eddies.

We did not find a consistent, overall pattern in the chlorophyll anomalies of coherent features as a function of age (Fig. 7). In the southeast province, winter-time cyclonic RCLVs have elevated chlorophyll relative to their surroundings- a signature that declines with age. In the Lee Eddy region, cyclones and anticyclones have strong positive chl-a anomalies relative to their surroundings, mostly independent of age, except in winter-time anticyclones for which the intensity of the anomaly grows significantly throughout eddy lifetimes.

4.1 Interpretation of Results with an Idealized Model

To interpret the comparisons of chl-a anomalies in SLA eddies and RCLVs, we consider the following idealized model that describes the biological and lateral mixing influences on the surface chl-a concentration in an eddy (B_{in}):

$$\frac{dB_{in}}{dt} = \mu B_{in} - \Psi(B_{in} - B_{out}). \tag{5}$$

B_{out} is the outside-eddy concentration, μ is the net biological rate of change (e.g., growth, mortality, photoacclimation) that may be driven by vertical processes, and Ψ is the lateral fluid exchange rate at the eddy boundary.

A coherent eddy minimizes Ψ, whereas a leaky eddy has a higher lateral fluid exchange rate with outside-eddy waters. In the simple case where trapping and leaky eddies have an equivalent net positive biological rate of change (μ) and a constant outside-eddy concentration (B_{out}), the coherent eddy will have a more positive $\frac{dB_{in}}{dt}$, promoting higher in-eddy concentrations (B_{in}). Indeed, the pattern generally observed across the NPSG domain is more positive chl-a anomalies in RCLVs (Figs. 3, 4).

In the northern province, the chl-a anomalies in RCLVs do not differ substantially from SLA eddies. When chl-a anomalies appear similar to the background for both types, such as in the spring (Fig. 5d), this indicates that broadly, eddies are not perturbing the nutrient environment in an influential way. When anomalies are positive in anticyclones in the winter (Fig. 5b), Eq. 5 suggests that the net population growth rate (μ) must be higher in SLA eddies than in coherent structures to maintain the same B_{in}. For example, lateral dilution in northern wintertime SLA anticyclones may drive higher growth rates or reduce the grazing pressure (Lehahn et al., 2017; Ser-Giacomi et al., 2023). When SLA eddies contain more positive anomalies than RCLVs, such as anticyclones in the northern summer and fall (Fig. 5f, h), potential mechanisms include increased vertical mixing associated with submesoscale filaments on eddy edges (Calil & Richards, 2010; Peterson et al., 2011; Mahadevan, 2016; F. Liu et al., 2017; L. Wang et al., 2018; Guo et al., 2019), eddy-eddy interactions (Guidi et al., 2012), wind interactions, or horizontal advection of chlorophyll-rich waters into the peripheries (Xu et al., 2019).

Some RCLVs have more negative chl-a anomalies than the background including both polarities in the northern fall (Fig. 5h), wintertime cyclones in the north (Fig. 5b), anticyclones in the northern summer (Fig. 5f), and southeastern anticyclones in the fall (Fig. 5i). According to Eq. 5, a decrease in chl-a concentration within an eddy (B_{in}) occurs when $\mu B_{in} < \Psi(B_{in} - B_{out})$. In a coherent eddy where Ψ is minimized, an anomalously low μ will result in lower chl-a. Low nutrient supply rates due to deeper density surfaces in anticyclones or high mortality may cause this. Alternatively, phytoplankton cells may decrease their chlorophyll-to-carbon ratio if light availability increases (Geider, 1987; MacIntyre et al., 2000) from shoaling isopycnals in the interior of cyclones. RCLVs may continue to harbor negative anomalies longer than SLA eddies because the chl-a deficit is shielded from mixing with surrounding waters.

Negative anomalies are more likely to occur in SLA eddy boundaries than their RCLV counterparts in some seasons in the Hawaiian Lee Eddy province (Fig. 6) and in cyclones in the northern fall (Fig. 5h). This could occur if the grazing pressure is higher on eddy edges than in the center, as found in some observations (Froneman & Perissinotto, 1996; Goldthwait & Steinberg, 2008; Gødo et al., 2012; Schmid et al., 2020).

4.2 Implications of Regional and Seasonal Variability

The overall influence of trapping in the gyre (Figs. 3, 4) is obscured because the differences in chl-a between RCLVs and SLA eddies are minimized in the north but maximized in the south. Furthermore, the magnitude and sign of satellite chl-a anomalies differ regionally and seasonally. This study highlights the NPSG, but Gaube et al. (2014) showed that the cross-correlation of sea surface height with chl-a anomalies is inconsistent across the global ocean. Similarly, we expect that the relative impacts of Lagrangian trapping on phytoplankton vary by location.

The Hawaiian Lee Eddies consistently form close to land, making them more accessible, and accordingly, have been heavily sampled. They have been presented as "representative" features of the open ocean (Falkowski et al., 1991; Olaizola et al., 1993; Bidi-

gare et al., 2003; Benitez-Nelson et al., 2007), but our results demonstrate that the chl-*a* signatures of the Lee Eddies differ considerably from eddies in the surrounding gyre. Hawaiian Lee Eddies of all types elevate chl-*a* more than any other subdomain, notably in wintertime anticyclones, with trapping further enhancing local hot spots of chl-*a*. Therefore the underlying mechanisms for the biological response to eddies in the north, southeast, and Hawaiian Lee regions of the NPSG may not be equivalent.

4.3 Interpretation of the Response to Eddy Age

We hypothesized that perturbations to surface chl-*a* would dilute as eddies age. However, we found a markedly varied pattern in the chl-*a* anomaly as a function of age for long-lived RCLVs that depends on the season and province. We again invoke a simple model to interpret these results, expanding upon Eq. 5.

The local anomaly (δc_{loc}; Eq. 3) compares the chl-*a* concentration inside an eddy (B_{in}) relative to the concentration in the eddy's immediate surroundings (B_{out}). The change in chl-*a* concentration outside of the eddy is

$$\frac{dB_{out}}{dt} = \mu B_{out} + \Psi \left(\frac{A_{in}}{A_{out}} \right) (B_{in} - B_{out}) \ , \tag{6}$$

where A_{in} is the area of the eddy and A_{out} is the area of the annulus from the eddy boundary to double the radius. In this simplified case, we neglect the influences of mixing with waters beyond the annulus, vertical processes, and acclimation of pigments.

The rate of change in δc_{loc} is

$$\frac{d}{dt}(\delta c_{loc}) = \frac{dB_{in}}{dt} - \frac{dB_{out}}{dt}. \tag{7}$$

Now consider the case where μ is equivalent inside and outside an eddy. This is more likely to occur toward the end of an eddy's life when perturbations due to eddy pumping and eddy-wind interactions are dampened (Huang et al., 2017). By assuming the feature is circular ($A_{in} = \pi r^2$), we substitute Eqs. 5 and 6 into Eq. 7:

$$\frac{d}{dt}(\delta c_{loc}) = (\mu - \frac{4}{3}\Psi)(B_{in} - B_{out}). \tag{8}$$

Intuitively, Eq. 8 indicates that a larger Ψ (i.e., a leakier boundary) will cause chl-*a* anomalies in eddies to dilute more rapidly (Fig. S10). A positive $\frac{d}{dt}(\delta c_{loc})$ is sustained when $\mu > \frac{4\Psi}{3}$ and $B_{in} > B_{out}$. Since chl-*a* is anomalously high in Hawaiian Lee RCLVs, these features are most likely to meet both conditions, consistent with the results of Fig. 7. In most cases, however, an eddy-associated chl-*a* anomaly will decay via lateral dilution without sustained net positive growth. In light of this, we suggest that the biological rate of change in the most isolated eddy environments tends to be on par or smaller than the dilution rate; anomalies stimulated in dispersive SLA eddies are diluted even faster.

4.4 Limitations and Future Investigation

Satellite-observed changes in chl-*a* at the mesoscale remain enigmatic concerning the underlying ecological dynamics because chlorophyll is not a direct measurement of phytoplankton biomass. For example, it is unknown whether elevated chl-*a* in wintertime subtropical gyre anticyclones is due to increased productivity (Dufois et al., 2016) or changes in the cellular chlorophyll-to-carbon ratio due to photoacclimation (Cornec et al., 2021; He et al., 2021; Strutton et al., 2023). While both can be true (Su et al., 2021), higher fish catch occurs in anticyclones compared to cyclones around the Hawaiian Islands (Arostegui et al., 2022) potentially suggesting that increased phytoplankton productivity supports higher trophic levels.

Changes in chl-a may also indicate a change in community structure. Waga et al. (2019) used a size structure ocean color algorithm to infer that anticyclones in subtropical gyres support larger phytoplankton cells than cyclonic eddies. Hernández-Carrasco et al. (2023) found that Lagrangian coherence promoted diatom blooms in the Mediterranean Sea, but to what extent phytoplankton community structure may differ in RCLVs and SLA eddies remains an open question. Further, a succession of phytoplankton types, as found in a model simulation of Hawaiian Lee Eddies (Friedrich et al., 2021), may underlie observed chl-a concentrations. Retrospective analysis of existing observations from eddies and targeted in situ campaigns would provide valuable insight into the relationship between eddy trapping and phytoplankton functional types.

Although satellites are the only ocean observing systems that obtain nearly full spatial coverage within days, a fundamental limitation is the restriction to the surface. Eddies affect subsurface chl-a in the NPSG by altering the depth of the deep chlorophyll maximum (Gaube et al., 2019; Xiu & Chai, 2020) and the vertical community structure (Olaizola et al., 1993; Brown et al., 2008; Fong et al., 2008; Barone et al., 2019). Therefore, the biological response to eddies at depth may differ from the surface signature (Huang & Xu, 2018; Zhao et al., 2021). The size of Lagrangian coherent boundaries may also change with depth (Nencioli et al., 2008; Ntaganou et al., 2023). Another limitation of satellite chl-a observations is missing data from cloud coverage including during storms, which can stimulate phytoplankton blooms in eddies (X. Liu et al., 2009; Shang et al., 2015; Villar et al., 2015; Chacko, 2017; Mikaelyan et al., 2020). Co-locating the bounds of RCLVs with autonomous vehicles and shipboard observations are promising avenues of future exploration to circumnavigate satellite limitations.

5 Conclusion

By co-locating satellite chl-a observations with two decades of Eulerian and Lagrangian coherent eddies in the NPSG, we show more positive chl-a anomalies are found within the bounds of RCLVs compared to SLA eddies. This is consistent with the hypothesis that lateral processes dilute local, recent changes to biomass in dispersive eddies. However, there are significant regional and seasonal differences within the NPSG, and trends in chl-a anomalies as a function of eddy age differ even in the most coherent features. Based on these results, we expect that the response to eddy trapping is variable across the global ocean due to the complexity of mesoscale biophysical interactions. Finally, we argue that the effects of lateral dilution and the diversity of trapping behaviors must be considered when evaluating biogeochemical states in eddies to accurately determine the contribution of mesoscale processes to global primary production.

Open Research Section

This study used CMEMS Level 4, 1/4° SLA and geostrophic velocity gridded global ocean dataset, Version 008_047 (CMEMS, 2020). The 8-day average chl-a product is produced by OC-CCI (Version 6.0) and distributed by the European Space Agency (Sathyendranath et al., 2019). We used the OceanEddies MATLAB software to detect and track Eulerian SLA eddy contours. The software was obtained from `https://github.com/ifrenger/OceanEddies` (last access: 13 October 2021). The OceanParcels v2.0 Python package was used to run Lagrangian particle simulations (Delandmeter & van Sebille, 2019). The figures were created with Matplotlib 3.3.4 (Caswell et al., 2021; Hunter, 2007).

The Python software developed for this study is available on GitHub and Zenodo (Jones-Kellett, 2023b). The NPSG RCLV dataset is publicly available, distributed by Simons CMAP at `https://simonscmap.com/catalog/datasets/RCLV_atlas_version2` (Jones-Kellett, 2024).

Acknowledgments

We thank Katy Abbott, Stephanie Dutkiewicz, and Enrico Ser-Giacomi for their feedback that greatly improved this manuscript. The Simons Foundation generously funded this project (SCOPE Award #329108, MJF; CBIOMES Award #549931, MJF).

Acronyms

Chl-*a* Chlorophyll-*a*
CMEMS Copernicus Marine Service
LAVD Lagrangian Averaged Vorticity Deviation
NPSG North Pacific Subtropical Gyre
OC-CCI Ocean Color Climate Change Initiative
RCLV Rotationally Coherent Lagrangian Vortex
SLA Sea Level Anomaly

References

Allen, C. B., Kanda, J., & Laws, E. A. (1996). New production and photosynthetic rates within and outside a cyclonic mesoscale eddy in the north pacific subtropical gyre. *Deep Sea Research Part I: Oceanographic Research Papers*, *43*, 917-936. doi: 10.1016/0967-0637(96)00022-2

Andrade-Canto, F., Karrasch, D., & Beron-Vera, F. J. (2020). Genesis, evolution, and apocalypse of loop current rings. *Physics of Fluids*, *32*(116603). doi: 10.1063/5.0030094

Arostegui, M. C., Gaube, P., Woodworth-Jefcoats, P. A., Kobayashi, D. R., & Braun, C. D. (2022). Anticyclonic eddies aggregate pelagic predators in a subtropical gyre. *Nature*, *609*, 535–540. doi: 10.1038/s41586-022-05162-6

Barone, B., Church, M. J., Dugenne, M., Hawco, N. J., Jahn, O., White, A. E., ... Karl, D. M. (2022). Biogeochemical dynamics in adjacent mesoscale eddies of opposite polarity. *Global Biogeochemical Cycles*, *36*(e2021GB007115). doi: 10.1029/2021GB007115

Barone, B., Coenen, A. R., Beckett, S. J., McGillicuddy, D. J., Jr., Weitz, J. S., & Karl, D. M. (2019). The ecological and biogeochemical state of the north pacific subtropical gyre is linked to sea surface height. *Journal of Marine Research*, *77*, 215-245. doi: 10.1357/002224019828474241

Bastine, D., & Feudel, U. (2010). Inhomogeneous dominance patterns of competing phytoplankton groups in the wake of an island. *Nonlinear Processes in Geophysics*, *17*, 715–731. doi: 10.5194/npg-17-715-2010

Benitez-Nelson, C. R., Bidigare, R. R., Dickey, T. D., Landry, M. R., Leonard, C. L., Brown, S. L., ... Yang, E. J. (2007). Mesoscale eddies drive increased silica export in the subtropical pacific ocean. *Science*, *316*, 1017-1021. doi: 10.1126/science.1136221

Beron-Vera, F. J., Hadjighasem, A., Xia, Q., Olascoaga, M. J., & Haller, G. (2019). Coherent lagrangian swirls among submesoscale motions. *PNAS*, *116*(37), 18251-18256. doi: 10.1073/pnas.1701392115

Beron-Vera, F. J., Wang, Y., Olascoaga, M. J., Goni, G. J., & Haller, G. (2013). Objective detection of oceanic eddies and the agulhas leakage. *Journal of Physical Oceanography*, *43*, 1426-1438. doi: 10.1175/JPO-D-12-0171.1

Bidigare, R. R., Benitez-Nelson, C., Leonard, C. L., Quay, P. D., Parsons, M. L., Foley, D. G., & Seki, M. P. (2003). Influence of a cyclonic eddy on microheterotroph biomass and carbon export in the lee of hawaii. *Geophysical Research Letters*, *30*(1318). doi: 10.1029/2002GL016393

Bracco, A., Provenzale, A., & Scheuring, I. (2000). Mesoscale vortices and the paradox of the plankton. *Proceedings: Biological Sciences*, *267*(1454), 1795-1800.

650 doi: 10.1098/rspb.2000.1212
651 Brown, S. L., Landry, M. R., Selph, K. E., Yang, E. J., Rii, Y. M., & Bidigare, R. R.
652 (2008). Diatoms in the desert: Plankton community response to a mesoscale
653 eddy in the subtropical north pacific. *Deep Sea Research Part II: Topical*
654 *Studies in Oceanography*, *55*, 1321-1333. doi: 10.1016/j.dsr2.2008.02.012
655 Calil, P. H. R., & Richards, K. J. (2010). Transient upwelling hot spots in the olig-
656 otrophic north pacific. *Journal of Geophysical Research*, *115*(C02003). doi: 10
657 .1029/2009JC005360
658 Calil, P. H. R., Richards, K. J., Jia, Y., & Bidigare, R. R. (2008). Eddy activity in
659 the lee of the hawaiian islands. *Deep-Sea Research II*, *55*, 1179-1194. doi: 10
660 .1016/j.dsr2.2008.01.008
661 Caswell, T. A., Droettboom, M., Lee, A., Sales de Andrade, E., Hunter, J., Firing,
662 E., & et al. (2021). *Matplotlib v3.3.4* [Software]. Zenodo. Retrieved from
663 `https://doi.org/10.5281/zenodo.4475376`
664 Chacko, N. (2017). Chlorophyll bloom in response to tropical cyclone hudhud in
665 the bay of bengal: Bio-argo subsurface observations. *Deep-Sea Research Part*
666 *I*, *124*, 66-72. doi: 10.1016/j.dsr.2017.04.010
667 Chaigneau, A., Eldin, G., & Dewitte, B. (2009). Eddy activity in the four major up-
668 welling systems from satellite altimetry (1992-2007). *Progress in Oceanography*,
669 *83*, 117-123. doi: 10.1016/j.pocean.2009.07.012
670 Chelton, D. B., DeSzoeke, R. A., Schlax, M. G., El Naggar, K., & Siwertz,
671 N. (1998). Geographic variability of the first baroclinic rossby radius
672 of deformation. *Journal of Physical Oceanography*, *28*, 433-460. doi:
673 10.1175/1520-0485(1998)028⟨0433:GVOTFB⟩2.0.CO;2
674 Chelton, D. B., Schlax, M. G., & Samelson, R. M. (2011). Global observations of
675 nonlinear mesoscale eddies. *Progress in Oceanography*, *91*, 167-216. doi: 10
676 .1016/j.pocean.2011.01.002
677 Chen, F., Cai, W.-J., Wang, Y., Rii, Y. M., Bidigare, R. R., & Benitez-Nelson, C. R.
678 (2008). The carbon dioxide system and net community production within a
679 cyclonic eddy in the lee of hawaii. *Deep-Sea Research II*, *55*, 1412-1425. doi:
680 10.1016/j.dsr2.2008.01.011
681 Clayton, S., Dutkiewicz, S., Jahn, O., & Follows, M. J. (2013). Dispersal, eddies,
682 and the diversity of marine phytoplankton. *Limnology and Oceanography: Flu-*
683 *ids and Environments*, *3*. doi: 10.1215/21573689-2373515
684 CMEMS. (2020). *Global ocean gridded l4 sea surface heights and derived variables*
685 *reprocessed 1993 ongoing, marine data store* [Dataset]. Copernicus Marine Ser-
686 vice. Retrieved from `https://doi.org/10.48670/moi-00148`
687 Condie, S., & Condie, R. (2016). Retention of plankton within ocean eddies. *Global*
688 *Ecology and Biogeography*, *25*, 1264-1277. doi: 10.1111/geb.12485
689 Cornec, M., Laxenaire, R., Speich, S., & Claustre, H. (2021). Impact of
690 mesoscale eddies on deep chlorophyll maxima. *Geophysical Research Letters*,
691 *48*(e2021GL093470). doi: 10.1029/2021GL093470
692 Delandmeter, P., & van Sebille, E. (2019). The parcels v2.0 lagrangian framework:
693 new field interpolation schemes. *Geoscientific Model Development*, *12*, 3571-
694 3584. doi: 10.5194/gmd-12-3571-2019
695 Denes, M. C., Froyland, G., & Keating, S. R. (2022). Persistence and material co-
696 herence of a mesoscale ocean eddy. *Physical Review Fluids*, *7*(034501). doi: 10
697 .1103/PhysRevFluids.7.034501
698 Dickey, T. D., Nencioli, F., Kuwahara, V. S., Leonard, C., Black, W., Rii, Y. M.,
699 ... Zhang, Q. (2008). Physical and bio-optical observations of oceanic cy-
700 clones west of the island of hawai'i. *Deep-Sea Research II*, *55*, 1195-1217. doi:
701 10.1016/j.dsr2.2008.01.006
702 d'Ovidio, F., De Monte, S., Alvain, S., Dandonneau, Y., & Levy, M. (2010). Fluid
703 dynamical niches of phytoplankton types. *PNAS*, *107*(43). doi: 10.1073/pnas
704 .1004620107

d'Ovidio, F., De Monte, S., Della Penna, A., Cotte, C., & Guinet, C. (2013). Ecological implications of eddy retention in the open ocean: a lagrangian approach. *Journal of Physics A: Mathematical and Theoretical*, *46*(254023). doi: 10.1088/1751-8113/46/25/254023

Dufois, F., Hardman-Mountford, N. J., Greenwood, J., Richardson, A. J., Feng, M., & Matear, R. J. (2016). Anticyclonic eddies are more productive than cyclonic eddies in subtropical gyres because of winter mixing. *Science Advances*, *2*(5). doi: 10.1126/sciadv.1600282

Faghmous, J. H., Frenger, I., Yao, Y., Warmka, R., Lindell, A., & Kumar, V. (2015). A daily global mesoscale ocean eddy dataset from satellite altimetry. *Scientific Data*, *2*(150028). doi: 10.1038/sdata.2015.28

Falkowski, P. G., Ziemann, D., Kolber, Z., & Bienfang, P. K. (1991). Role of eddy pumping in enhancing primary production in the ocean. *Nature*, *352*, 55–58. doi: 10.1038/352055a0

Fennel, K. (2001). The generation of phytoplankton patchiness by mesoscale current patterns. *Ocean Dynamics*, *52*, 58-70. doi: 10.1007/s10236-001-0007-y5

Fong, A. A., Karl, D. M., Lukas, R., Letelier, R. M., Zehr, J. P., & Church, M. J. (2008). Nitrogen fixation in an anticyclonic eddy in the oligotrophic north pacific ocean. *The ISME Journal*, *2*, 663-676. doi: 10.1038/ismej.2008.22

Friedrich, T., Powell, B. S., Stock, C. A., Hahn-Woernle, L., Dussin, R., & Curchitser, E. N. (2021). Drivers of phytoplankton blooms in hawaii: A regional model study. *Journal of Geophysical Research: Oceans*, *126*(e2020JC017069). doi: 10.1029/2020JC017069

Froneman, P. W., & Perissinotto, R. (1996). Structure and grazing of the microzooplankton communities of the subtropical convergence and a warm-core eddy in the atlantic sector of the southern ocean. *Marine Ecology Progress Series*, *135*, 237-245. doi: 10.3354/meps135237

Gaube, P., Chelton, D. B., Strutton, P. G., & Beherenfeld, M. J. (2013). Satellite observations of chlorophyll, phytoplankton biomass, and ekman pumping in nonlinear mesoscale eddies. *Journal of Geophysical Research: Oceans*, *118*, 6349-6370. doi: 10.1002/2013JC009027

Gaube, P., McGillicuddy Jr., D. J., Chelton, D. B., Behrenfeld, M. J., & Strutton, P. G. (2014). Regional variations in the influence of mesoscale eddies on near-surface chlorophyll. *Journal of Geophysical Research: Oceans*, *119*, 8195-8220. doi: 10.1002/2014JC010111

Gaube, P., McGillicuddy Jr., D. J., & Moulin, A. J. (2019). Mesoscale eddies modulate mixed layer depth globally. *Geophysical Research Letters*, *46*, 1505-1512. doi: 10.1029/2018GL080006

Geider, R. J. (1987). Light and temperature dependence of the carbon to chlorophyll a ratio in microalgae and cyanobacteria: implications for physiology and growth of phytoplankton. *New Phytologist*, *106*, 1-34. doi: 10.1111/j.1469-8137.1987.tb04788.x

Glover, D. M., Wroblewski, J. S., & McClain, C. R. (1994). Dynamics of the transition zone in coastal zone color scanner-sensed ocean color in the north pacific during oceanographic spring. *Journal of Geophysical Research: Oceans*, *99*(C4), 7501-7511. doi: 10.1029/93JC02144

Gødo, O. R., Samuelsen, A., Macaulay, G. J., Patel, R., Hjøllo, S. S., Horne, J., ... Johannessen, J. A. (2012). Mesoscale eddies are oases for higher trophic marine life. *PLoS ONE*, *7*(e30161). doi: 10.1371/journal.pone.0030161

Goldthwait, S. A., & Steinberg, D. K. (2008). Elevated biomass of mesozooplankton and enhanced fecal pellet flux in cyclonic and mode-water eddies in the sargasso sea. *Deep-Sea Research II*, *55*, 1360-1377. doi: 10.1016/j.dsr2.2008.01.003

Gower, J. F. R., Denman, K. L., & Holyer, R. J. (1980). Phytoplankton patchiness indicates the fluctuation spectrum of mesoscale oceanic structure. *Nature*, *288*,

157–159. doi: 10.1038/288157a0

Guidi, L., Calil, P. H. R., Duhamel, S., Björkman, K. M., Doney, S. C., Jackson, G. A., ... Karl, D. M. (2012). Does eddy-eddy interaction control surface phytoplankton distribution and carbon export in the north pacific subtropical gyre? *Journal of Geophysical Research*, *117*(G02024). doi: 10.1029/2012JG001984

Guo, M., Xiu, P., Chai, F., & Xue, H. (2019). Mesoscale and submesoscale contributions to high sea surface chlorophyll in subtropical gyres. *Geophysical Research Letters*, *46*(22), 13217–13226. doi: 10.1029/2019GL085278

Haller, G. (2015). Lagrangian coherent structures. *Annual Review of Fluid Mechanics*, *47*, 137-162. doi: 10.1146/annurev-fluid-010313-14132

Haller, G., & Beron-Vera, F. J. (2013). Coherent lagrangian vortices: the black holes of turbulence. *Journal of Fluid Mechanics*, *731*(R4). doi: 10.1017/jfm.2013.391

Haller, G., Hadjighasem, A., Farazmand, M., & Huhn, F. (2016). Defining coherent vortices objectively from the vorticity. *Journal of Fluid Mechanics*, *795*, 136-173. doi: 10.1017/jfm.2016.151

Harke, M. J., Frischkorn, K. R., Hennon, G. M. M., Haley, S. T., Barone, B., Karl, D. M., & Dyhrman, S. T. (2021). Microbial community transcriptional patterns vary in response to mesoscale forcing in the north pacific subtropical gyre. *Environmental Microbiology*, *23*(8), 4807-4822. doi: 10.1111/1462-2920.15677

He, Q., Tian, F., Yang, X., & Chen, G. (2022). Lagrangian eddies in the northwestern pacific ocean. *Journal of Oceanology and Limnology*, *40*(1), 66-77. doi: 10.1007/s00343-021-0392-7

He, Q., Zhan, H., Cai, S., & Zha, G. (2016). On the asymmetry of eddy-induced surface chlorophyll anomalies in the southeastern pacific: The role of eddy-ekman pumping. *Progress in Oceanography*, *141*, 202-211. doi: 10.1016/j.pocean.2015.12.012

He, Q., Zhan, H., Cai, S., & Zhan, W. (2021). Eddy-induced near-surface chlorophyll anomalies in the subtropical gyres: Biomass or physiology? *Geophysical Research Letters*, *48*(e2020GL091975). doi: 10.1029/2020GL091975

Hernández-Carrasco, I., Rossi, V., Navarro, G., Turiel, A., Bracco, A., & Orfila, A. (2023). Flow structures with high lagrangian coherence rate promote diatom blooms in oligotrophic waters. *Geophysical Research Letters*, *50*(e2023GL103688). doi: 10.1029/2023GL103688

Huang, J., & Xu, F. (2018). Observational evidence of subsurface chlorophyll response to mesoscale eddies in the north pacific. *Global Biogeochemical Cycles*, *45*, 8462-8470. doi: 10.1029/2018GL078408

Huang, J., Xu, F., Zhou, K., Xiu, P., & Lin, Y. (2017). Temporal evolution of near-surface chlorophyll over cyclonic eddy lifecycles in the southeastern pacific. *Journal of Geophysical Research: Oceans*, *122*, 6165-6179. doi: 10.1002/2017JC012915

Hunter, J. D. (2007). Matplotlib: A 2d graphics environment. *Computing in Science & Engineering*, *9*(3), 90-95. doi: 10.1109/MCSE.2007.55

Jones-Kellett, A. E. (2023a). *North pacific subtropical gyre rclv atlas (version 1)* [Dataset]. Zenodo. Retrieved from `https://doi.org/10.5281/zenodo.8139149`

Jones-Kellett, A. E. (2023b). *Rclvatlas* [Software]. Zenodo. Retrieved from `https://doi.org/10.5281/zenodo.7702978`

Jones-Kellett, A. E. (2024). *North pacific subtropical gyre rclv atlas (version 2)* [Dataset]. Zenodo. Retrieved from `https://doi.org/10.5281/zenodo.10849221`

Jones-Kellett, A. E., & Follows, M. J. (2024). A lagrangian coherent eddy atlas for biogeochemical applications in the north pacific subtropical gyre. *Earth System*

Science Data, *16*, 1475-1501. doi: 10.5194/essd-16-1475-2024

Karl, D. M., & Church, M. J. (2017). Ecosystem structure and dynamics in the north pacific subtropical gyre: New views of an old ocean. *Ecosystems*, *20*, 433-457. doi: 10.1007/s10021-017-0117-0

Katsanoulis, S., Farazmand, M., Serra, M., & Haller, G. (2020). Vortex boundaries as barriers to diffusive vorticity transport in two-dimensional flows. *Physical Review Fluids*, *5*(024701). doi: 10.1103/PhysRevFluids.5.024701

Landry, M. R., Brown, S. L., Rii, Y. M., Selph, K. E., Bidigare, R. R., Yang, E. J., & Simmons, M. P. (2008). Depth-stratified phytoplankton dynamics in cyclone opal, a subtropical mesoscale eddy. *Deep-Sea Research II*, *55*, 1348-1359. doi: 10.1016/j.dsr2.2008.02.001

Lehahn, Y., d'Ovidio, F., & Koren, I. (2018). A satellite-based lagrangian view on phytoplankton dynamics. *Annual Review of Marine Science*, *10*, 99-119. doi: 10.1146/annurev-marine-121916-063204

Lehahn, Y., d'Ovidio, F., Lévy, M., Amitai, Y., & Heifetz, E. (2011). Long range transport of a quasi isolated chlorophyll patch by an agulhas ring. *Geophysical Research Letters*, *38*(L16610). doi: 10.1029/2011GL048588

Lehahn, Y., Koren, I., Sharoni, S., d'Ovidio, F., Vardi, A., & Boss, E. (2017). Dispersion/dilution enhances phytoplankton blooms in low-nutrient waters. *Nature Communications*, *8*(14868). doi: 10.1038/ncomms14868

Lévy, M., Jahn, O., Dutkiewicz, S., & Follows, M. J. (2014). Phytoplankton diversity and community structure affected by oceanic dispersal and mesoscale turbulence. *Limnology and Oceanography: Fluids and Environments*, *4*, 67-84. doi: 10.1215/21573689-2768549

Lévy, M., Jahn, O., Dutkiewicz, S., Follows, M. J., & d'Ovidio, F. (2015). The dynamical landscape of marine phytoplankton diversity. *Journal of the Royal Society Interface*, *12*(20150481). doi: 10.1098/rsif.2015.0481

Liu, F., Tang, S., Huang, R. X., & Yin, K. (2017). The asymmetric distribution of phytoplankton in anticyclonic eddies in the western south china sea. *Deep-Sea Research Part I*, *120*, 29-38. doi: 10.1016/j.dsr.2016.12.010

Liu, T., Abernathey, R., Sinha, A., & Chen, D. (2019). Quantifying eulerian eddy leakiness in an idealized model. *Journal of Geophysical Research: Oceans*, *124*, 8869-8886. doi: 10.1029/2019JC015576

Liu, T., He, Y., Zhai, X., & Liu, X. (2022). Diagnostics of coherent eddy transport in the south china sea based on satellite observations. *Remote Sensing*, *14*(1690). doi: 10.3390/rs14071690

Liu, X., Wang, M., & Shi, W. (2009). A study of a hurricane katrina–induced phytoplankton bloom using satellite observations and model simulations. *Journal of Geophysical Research*, *114*(C03023). doi: 10.1029/2008JC004934

Liu, Y., Dong, C., Guan, Y., Chen, D., McWilliams, J., & Nencioli, F. (2012). Eddy analysis in the subtropical zonal band of the north pacific ocean. *Deep-Sea Research I*, *68*, 54-67. doi: 10.1016/j.dsr.2012.06.001

Lumpkin, C. (1998). *Eddies and currents of the hawaiian islands* (Unpublished doctoral dissertation). School of Ocean and Earth Science and Technology, University of Hawaii, Manoa.

MacIntyre, H. L., Kana, T. M., & Geider, R. J. (2000). The effect of water motion on short-term rates of photosynthesis by marine phytoplankton. *Trends in Plant Science*, *5*(1), 12-17. doi: 10.1016/S1360-1385(99)01504-6

Mahadevan, A. (2016). The impact of submesoscale physics on primary productivity of plankton. *Annual Review of Marine Science*, *8*, 161-184. doi: 10.1146/annurev-marine-010814-015912

McAndrew, P. M., Bidigare, R. R., & Karl, D. M. (2008). Primary production and implications for metabolic balance in hawaiian lee eddies. *Deep-Sea Research II*, *55*, 1300-1309. doi: 10.1016/j.dsr2.2008.01.004

McGillicuddy Jr., D. J. (2016). Mechanisms of physical-biological-biogeochemical in-

teraction at the oceanic mesoscale. *Annual Review of Marine Science*, *8*, 125-159. doi: 10.1146/annurev-marine-010814-015606

Mikaelyan, A. S., Mosharov, S. A., Kubryakov, A. A., Pautova, L. A., Fedorov, A., & Chasovnikov, V. K. (2020). The impact of physical processes on taxonomic composition, distribution and growth of phytoplankton in the open black sea. *Journal of Marine Systems*, *208*(103368). doi: 10.1016/j.jmarsys.2020.103368

Nencioli, F., Kuwahara, V. S., Dickey, T. D., Rii, Y. M., & Bidigare, R. R. (2008). Physical dynamics and biological implications of a mesoscale eddy in the lee of hawai'i: Cyclone opal observations during e-flux iii. *Deep-Sea Research II*, *55*, 1252-1274. doi: 10.1016/j.dsr2.2008.02.003

Nicholson, D., Emerson, S., & Eriksen, C. C. (2008). Net community production in the deep euphotic zone of the subtropical north pacific gyre from glider surveys. *Limnology and Oceanography*, *53*(5), 2226-236. doi: 10.4319/lo.2008.53.5_part_2.2226

Ntaganou, N., Kourafalou, V., Beron-Vera, F., Olascoaga, M., Le Hénaff, M., & Androulidakis, Y. (2023). Influence of caribbean eddies on the loop current system evolution. *Frontiers in Marine Science*, *10*(961058). doi: 10.3389/fmars.2023.961058

Olaizola, M., Ziemann, D. A., Bienfang, P. K., Walsh, W. A., & Conquest, L. D. (1993). Eddy-induced oscillations of the pycnocline affect the floristic composition and depth distribution of phytoplankton in the subtropical pacific. *Marine Biology*, *116*, 533-542. doi: 10.1007/BF00355471

Perruche, C., Rivière, P., Lapeyre, G., Carton, X., & Pondaven, P. (2011). Effects of surface quasi-geostrophic turbulence on phytoplankton competition and coexistence. *Journal of Marine Research*, *69*, 105-135. doi: 10.1357/002224011798147606

Peterson, T. D., Crawford, D. W., & Harrison, P. J. (2011). Evolution of the phytoplankton assemblage in a long-lived mesoscale eddy in the eastern gulf of alaska. *Marine Ecology Progress Series*, *424*, 53-73. doi: 10.3354/meps08943

Provenzale, A. (1999). Transport by coherent barotropic vortices. *Annual Review of Fluid Mechanics*, *31*, 55-93. doi: 10.1146/annurev.fluid.31.1.55

Rii, Y. M., Brown, S. L., Nencioli, F., Kuwahara, V., Dickey, T., Karl, D. M., & Bidigare, R. R. (2008). The transient oasis: Nutrient-phytoplankton dynamics and particle export in hawaiian lee cyclones. *Deep Sea Research Part II: Topical Studies in Oceanography*, *55*, 1275-1290. doi: 10.1016/j.dsr2.2008.01.013

Sathyendranath, S., Brewin, R. J. W., Brockmann, C., Brotas, V., Calton, B., Chuprin, A., ... Platt, T. (2019). An ocean-colour time series for use in climate studies: the experience of the ocean-colour climate change initiative (oc-cci). *Sensors*, *19*(4285). doi: 10.3390/s19194285

Schmid, M. S., Cowen, R. K., Robinson, K., Luo, J. Y., Briseo-Avena, & Spongaugle, S. (2020). Prey and predator overlap at the edge of a mesoscale eddy: fine-scale, in-situ distributions to inform our understanding of oceanographic processes. *Scientific Reports*, *10*(921). doi: 10.1038/s41598-020-57879-x

Seki, M. P., Polovina, J. J., Brainard, R. E., Bidigare, R. R., Leonard, C. L., & Foley, D. G. (2001). Biological enhancement at cyclonic eddies tracked with goes thermal imagery in hawaiian waters. *Geophysical Research Letters*, *28*(8), 1583-1586. doi: 10.1029/2000GL012439

Ser-Giacomi, E., Martinez-Garcia, R., Dutkiewicz, S., & Follows, M. J. (2023). A lagrangian model for drifting ecosystems reveals heterogeneity-driven enhancement of marine plankton blooms. *Nature Communications*, *14*(6092). doi: 10.1038/s41467-023-41469-2

Shang, X., Zhu, H., Chen, G., Xu, C., & Yang, Q. (2015). Research on cold core eddy change and phytoplankton bloom induced by typhoons: Case studies in the south china sea. *Advances in Meteorology*, *2015*(340432). doi: 10.1155/2015/340432

Strutton, P. G., Trull, T. W., Phillips, H. E., Duran, E. R., & Pump, S. (2023). Biogeochemical argo floats reveal the evolution of subsurface chlorophyll and particulate organic carbon in southeast indian ocean eddies. *Journal of Geophysical Research: Oceans*, *128*(e2022JC018984). doi: 10.1029/2022JC018984

Su, J., Strutton, P. G., & Schallenberg, C. (2021). The subsurface biological structure of southern ocean eddies revealed by bgc-argo floats. *Journal of Marine Systems*, *220*(103569). doi: 10.1016/j.jmarsys.2021.103569

Tarshish, N., Abernathey, R., Zhang, C., Dufour, C. O., Frenger, I., & Griffies, S. M. (2018). Identifying lagrangian coherent vortices in a mesoscale ocean model. *Ocean Modelling*, *130*, 15-28. doi: 10.1016/j.ocemod.2018.07.001

Travis, S., & Qiu, B. (2020). Seasonal reversal of the near-surface chlorophyll response to the presence of mesoscale eddies in the south pacific subtropical countercurrent. *Journal of Geophysical Research: Oceans*, *125*(e2019JC015752). doi: 10.1029/2019JC015752

Vaillancourt, R. D., Marra, J., Seki, M. P., Parsons, M. L., & Bidigare, R. R. (2003). Impact of a cyclonic eddy on phytoplankton community structure and photosynthetic competency in the subtropical north pacific ocean. *Deep-Sea Research I*, *50*, 829-847. doi: 10.1016/S0967-0637(03)00059-1

Vaz, A. C., Richards, K. J., Jia, Y., & Paris, C. B. (2013). Mesoscale flow variability and its impact on connectivity for the island of hawai'i. *Geophysical Research Letters*, *40*, 332-337. doi: 10.1029/2012GL054519

Villar, E., Farrant, G., Follows, M., Garczarek, L., Speich, S., Audic, S., ... Iudicone, D. (2015). Environmental characteristics of agulhas rings affect interocean plankton transport. *Science*, *348*(6237). doi: 10.1126/science.1261447

Vortmeyer-Kley, R., Lünsmann, B., Berthold, M., Gräwe, U., & Feudel, U. (2019). Eddies: Fluid dynamical niches or transporters? - a case study in the western baltic sea. *Frontiers in Marine Science*, *6*(118). doi: 10.3389/fmars.2019.00118

Waga, H., Hirawake, T., & Ueno, H. (2019). Impacts of mesoscale eddies on phytoplankton size structure. *Geophysical Research Letters*, *46*(13), 191-198. doi: 10.1029/2019GL085150

Wang, L., Huang, B., Laws, E. A., Zhou, K., Liu, X., Xie, Y., & Dai, M. (2018). Anticyclonic eddy edge effects on phytoplankton communities and particle export in the northern south china sea. *Journal of Geophysical Research: Oceans*, *123*, 7632-7650. doi: 10.1029/2017JC013623

Wang, Y., Olascoaga, M. J., & Beron-Vera, F. J. (2015). Coherent water transport across the south atlantic. *Geophysical Research Letters*, *42*, 4072-4079. doi: 10.1002/2015GL064089

Woods, J. D., & Onken, R. (1982). Diurnal variation and primary production in the ocean — preliminary results of a lagrangian ensemble model. *Journal of Plankton Research*, *4*(3). doi: 10.1093/plankt/4.3.735

Xiu, P., & Chai, F. (2020). Eddies affect subsurface phytoplankton and oxygen distributions in the north pacific subtropical gyre. *Geophysical Research Letters*, *47*(15). doi: 10.1029/2020GL087037

Xu, G., Dong, C., Liu, Y., Gaube, P., & Yang, J. (2019). Chlorophyll rings around ocean eddies in the north pacific. *Scientific Reports*, *9*(2056). doi: 10.1038/s41598-018-38457-8

Yoshida, S., Qiu, B., & Hacker, P. (2010). Wind-generated eddy characteristics in the lee of the island of hawaii. *Journal of Geophysical Research*, *115*(C03019). doi: 10.1029/2009JC005417

Zhao, D., Xu, Y., Zhang, X., & Huang, C. (2021). Global chlorophyll distribution induced by mesoscale eddies. *Remote Sensing of Environment*, *254*(112245). doi: 10.1016/j.rse.2020.112245

Zhou, K., Benitez-Nelson, C. R., Huang, J., Xiu, P., Sun, Z., & Dai, M. (2021). Cyclonic eddies modulate temporal and spatial decoupling of particulate car-

bon, nitrogen, and biogenic silica export in the north pacific subtropical gyre. *Limnology and Oceanography*, *66*(9). doi: 10.1002/lno.11895